J. COMBIN. MATH. COMBIN. COMPUT. 127a (2025) 2913--2932

Journal of Combinatorial Mathematics
and Combinatorial Computing
www.combinatorialpress.com/jcmcc

Path Optimization and Decision Making Mechanism for Driverless Vehicles in Intelligent Transportation Systems under Vehicle-Circuit Collaboration

Weijian Li[1], Jigui Liang[1,✉], Chunyi Yu[1], Jianfei Wang[2]

[1] *Qujing Xuanfu Highway Investment and Construction Development Co., Ltd., Qujing, Yunnan, 655000, China*

[2] *Yunnan Construction and Investment Holding Group Co., Ltd., Kunming, Yunnan, 650500, China*

ABSTRACT

In this study, we construct an unmanned vehicle path optimization model based on fast extended random tree, and after kinematic modeling of unmanned vehicles, we introduce the artificial potential field method to improve the fast extended random tree algorithm, and apply it to the path optimization of unmanned vehicles. According to the swarm intelligence perception decision-making algorithm, the end-to-end unmanned vehicle decision-making model based on vehicle-circuit collaboration is constructed. The effectiveness of this paper's driverless path optimization and decision-making model based on vehicle-circuit collaboration is examined. The waiting time for red light of this paper's model is shorter than other path planning schemes, and the vehicle passing benefit at intersections is the highest. The passing benefit values of this paper's model are 70.3% and 46.8% higher than Maxband scheme and Synchro scheme, respectively. In the right-turn simulation experiments, the main vehicle speed change shows a tendency to accelerate and the path is basically overlapped with the edge of the lane without offsetting the center of the lane. In the normal driving speeds of [14,38], the fuel consumption of the driverless vehicle shows an up and down trend, and the carbon dioxide emission varies with the fuel consumption. The total cost of traveling decreases with increasing speed.

Keywords: improved fast scaling random tree, swarm intelligence perceptual decision making, vehicle-road collaboration technique, path optimization, driverless

1. Introduction

With the continuous development of science and technology and people's requirements for traffic safety continue to improve, driverless technology has gradually become a hot spot of people's attention. As a key technology in the field of intelligent transport in recent years, unmanned technology realises autonomous driving without human control by using sensors, computer vision

✉ Corresponding author.
E-mail address: 17665719586@163.com (J. Liang).

Received 12 January 2024; Revised 15 March 2024; Accepted 20 November 2024; Published Online 15 April 2025.
DOI: 10.61091/jcmcc127a-165

and other scientific and technological means [1-3]. The intelligent path optimisation and decision-making mechanism in unmanned driving is considered to be the core of unmanned driving, which directly affects the safety, efficiency and user experience of vehicle driving [4-5].

Path optimisation refers to finding the optimal route by using mathematical tools and techniques such as algorithms, graph theory, genetic algorithms, etc. under the premise of satisfying driving safety and efficiency. In unmanned vehicles, path optimisation is a key step to achieve automatic navigation, and its performance directly affects the driving effect and safety performance of the vehicle. Driverless vehicles need to choose the optimal path under different road conditions according to different travelling needs [6-9]. In order to ensure safety and efficiency, path optimisation needs to take into account factors such as road traffic conditions and travel restrictions, as well as attempting to maximise passenger comfort and energy savings. Decision-making mechanism is a mechanism by which driverless vehicles make appropriate decisions such as accelerating, decelerating, overtaking, etc. based on perceived environmental information [10-13]. The accuracy and timeliness of decision-making directly affects the safety and efficiency of the vehicle. Intelligent path optimisation and decision-making is a crucial part of driverless systems, which can ensure the safe and efficient operation of vehicles and provide passengers with better travel experiences [14-16].

Path optimisation lies in finding the path points that are free of obstacles and can reach the destination, and path optimisation of a driverless vehicle is a complex and critical technical field. From sensing, decision-making to control, each link requires a high degree of intelligence and collaborative cooperation in order to achieve safe and efficient autonomous driving. Literature [17] introduces an integrated approach of multi-stage model and improved genetic algorithm to obtain the optimal delivery plan for driverless vehicles based on the factors affecting path optimisation such as load capacity and traffic conditions encountered by the self-driving vehicles. Experimental results proved the existence of advantages of this plan. Literature [18] proposes combining the improved artificial potential field method with RRT algorithm for path planning, aiming to improve the efficiency of path optimisation. The improved artificial potential field method is combined and modelled with a vehicle kinematics model and an MPC trajectory tracking controller with constraints is designed to verify the advantages and disadvantages of the path. The experimental results are feasible and the method can achieve optimised paths according to with different environments and vehicle states. Literature [19] stated that driverless vehicles fundamentally transform the control of traditional cars, it uses technology to improve the safety and efficiency of the transport system, and path optimisation is a key technology for driverless vehicles. The original algorithm has been improved by ant colony algorithm, which can be done to deal with the emergency conditions of the road situation. Literature [20] investigates the method of automatic path optimisation for driverless vehicles based on ant colony algorithm. Based on the existing literature and knowledge of the field, a path optimisation method for human-driven vehicles with improved ant colony algorithm is designed and validated, and the results show that the method has excellent adaptive properties.

The decision-making mechanism of driverless vehicles is one of the core technologies to achieve autonomous driving. Through the three links of perception, judgement and decision-making, it can achieve the ability to perceive the surrounding environment of the vehicle, judge the state of the vehicle and make corresponding decisions to ensure the safe driving of the vehicle. Literature [21] introduced road conditions into the driving decision-making mechanism and designed a decision-making mechanism for self-driving vehicles based on the SVR model using weighted hybrid kernel function and particle swarm optimisation algorithm for optimisation. By quantitatively analysing the effect of road conditions on driving decisions, it is concluded that the performance of the decision-making mechanism is positively affected by road conditions. Literature [22] highlights a decision-making framework based on hierarchical state machines and with a three-layer finite state machine decision-making system structure, each of whose layers has a unique function. Simulation experiments pointed out that the strategy can integrate multiple criteria and is able to evaluate the energy efficiency values of vehicle states in real time, achieving optimal decision-making choices. Literature [23] addresses the difficulty of making timely and accurate decisions for self-driving vehicles in highly dynamic traffic environments. And proposed RSAN as a method to improve the decision making of self-driving vehicles learning from excellent human drivers, and simulation experiments verified that the method has a faster convergence speed and better decision-making accuracy. Literature [24] introduces new integrated threat assessment algorithms for decision-making systems. An interaction multiple model is used to predict the surrounding vehicle motion, consider its potential threats, and construct a comprehensive threat assessment function to evaluate the threats in each state. Simulation experiments reveal that the presented algorithm not only facilitates self-driving vehicles to determine safe trajectories in real time, but also maintains good manoeuvrability.

The article takes vehicle-circuit collaboration technology as the underlying logic of the model, and after kinematic modeling of unmanned vehicles, uses the improved fast extended random tree algorithm to optimize the driving path of unmanned vehicles, and constructs the unmanned vehicle path optimization model based on fast extended random tree. Based on the swarm intelligence perception decision-making algorithm, the unmanned decision-making network structure is designed to construct the end-to-end unmanned decision-making model based on vehicle-circuit collaboration. And then, in order to test the effectiveness of this paper's model, analyze the optimization results and optimization paths of this paper's model in path optimization simulation experiments. Finally, the driving cost of this paper's model in optimizing the driverless car is further analyzed.

2. Driverless Path Optimization and Decision Making Model Based on Vehicle-Circuit Collaboration

2.1. Vehicle-Road Collaboration Technology

2.1.1. Theory of Vehicle-Road Collaboration Technology. Intelligent transportation is regarded as the future development direction in the field of transportation at home and abroad, and vehicle-road collaboration technology is the main point of development in the field of intelligent transportation in recent years [25]. Vehicle-Road Collaboration refers to an intelligent transportation system that realizes collaborative decision-making between vehicle-vehicle (V2V) or vehicle-road (V2I) based on the vehicle network direct-connection communication technology (V2X). Vehicles in this environment can exchange information and data between vehicle and vehicle, vehicle and road. Currently, the mainstream vehicle-road collaboration technology in the industry is Cellular Vehicular Networking (C-V2X) direct connection communication technology, including LTE-V2X and 5G-V2X, and supports the smooth evolution of LTE-V2X to 5G-V2X. Vehicle-Road Collaboration (VRC) technology can realize real-time collection and integration of traffic information, active safety control of vehicles and collaborative management of roads, ensure the safety of vehicle traffic, improve the efficiency of traffic, and then form a kind of safe and efficient intelligent transportation system.

2.1.2. Vehicle-road cooperative systems. The cooperative vehicle-road system (CVIS) is a subsystem of the intelligent transportation system (ITS), and the architecture of the CVIS is shown in Fig. 1, which mainly contains the intelligent vehicle-based system, the roadside system, and the vehicle. The main role of the intelligent vehicle system is perception, which is composed of vehicle information acquisition system, control unit and wireless communication equipment. Among them, the information acquisition system is mainly used for the information acquisition of the vehicle itself and the vehicle traveling process. The control unit is mainly used to control the vehicle operation status and human-computer interaction and other functions. Wireless communication equipment is mainly used to receive all kinds of information sent by roadside equipment and other vehicles. The main role of the roadside system is to integrate and organize all kinds of traffic information data, which is mainly composed of roadside information acquisition system, control unit and wireless communication equipment. The roadside information acquisition system is based on various sensors, and real-time acquisition of traffic flow and other status information is carried out through the sensors. The roadside control unit is responsible for coordinating the orderly operation of the entire vehicle and road system. The wireless communication equipment is responsible for information interaction with vehicles and other equipment.

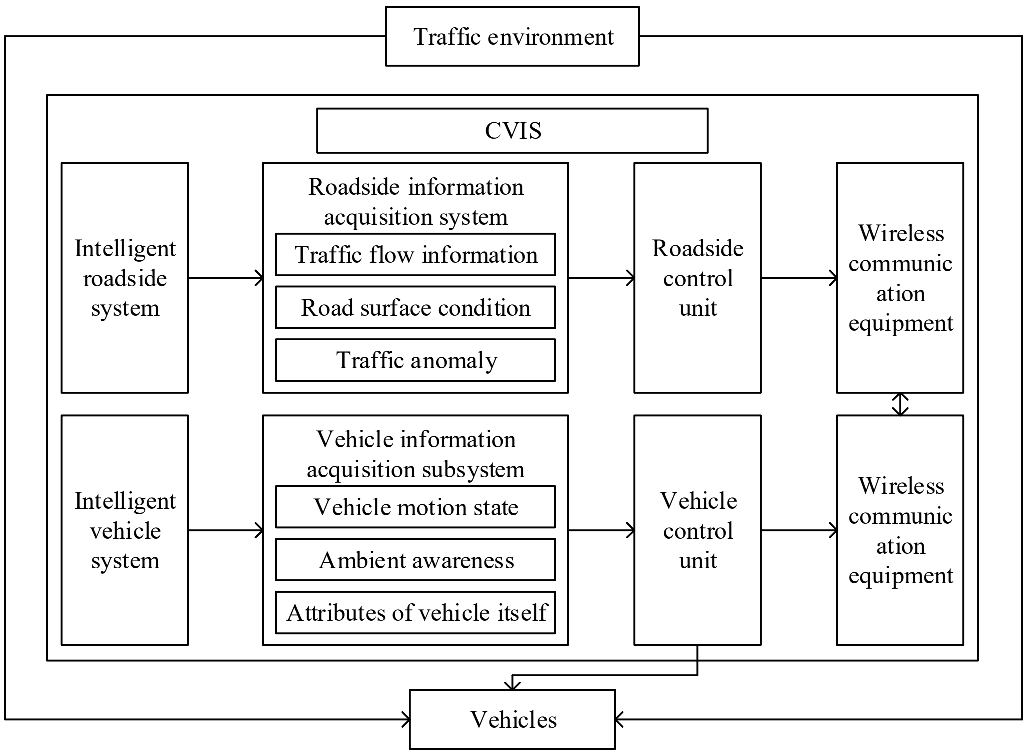

Fig. 1. Coordinated vehicle-infrastructure system structure

2.2. *Unmanned Vehicle Path Optimization Based on Fast Expanding Random Trees*

2.2.1. Unmanned Vehicle Kinematic Modeling. Kinematics is the study of the laws of motion of objects from a geometric perspective, including the corresponding changes in variables such as velocity and position of an object in three-dimensional space over time. Incorporating the kinematic model of the vehicle in the vehicle path planning algorithm can make the path obtained from planning more feasible.

The vehicle steering model is shown in Fig. 2. In the inertial coordinate system OXY, the axle center coordinate of the front axle of the vehicle is (X_f, Y_f), and the axle center coordinate of the rear axle of the vehicle is (X_r, Y_r). φ is the heading angle of the vehicle during driving, i.e., the traverse angle of the vehicle, φ_f is the deflection angle of the front wheels when the vehicle turns, υ_τ is the center velocity of the rear axle of the vehicle during driving, υ_τ is the center velocity of the front axle of the vehicle during driving, and 1 is the axle distance.

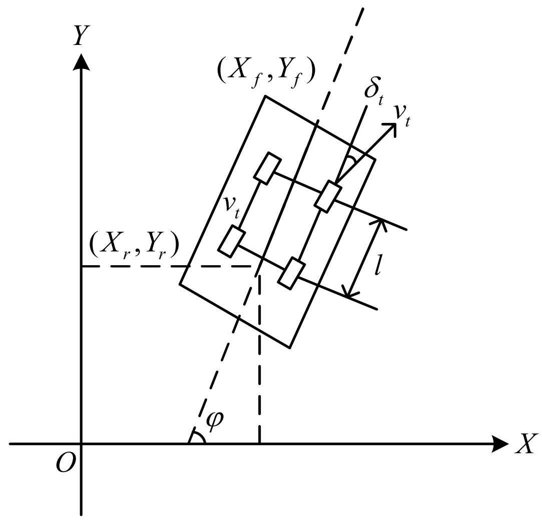

Fig. 2. Vehicle motion model

The front wheel steering process of the vehicle during driving is shown in Fig. 3, R represents the rear wheel steering radius of the vehicle, P is the instantaneous center of rotation of the vehicle, M is the rear axle axis of the vehicle, and N is the front axle axis. Here it is assumed that the lateral deflection angle of the center of mass of the vehicle is constant and does not change during vehicle driving, i.e., the instantaneous steering radius of the vehicle and the radius of curvature of the road are the same.

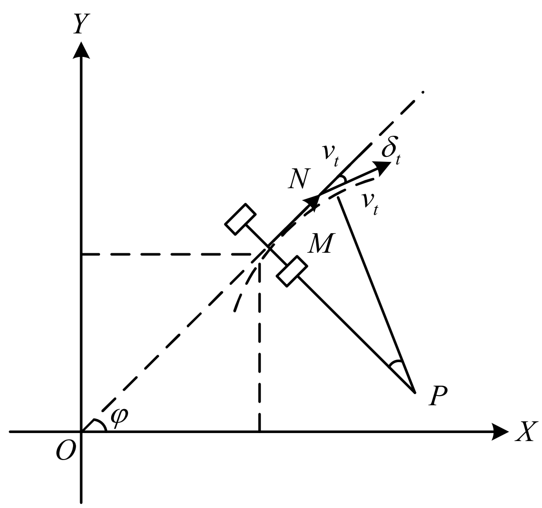

Fig. 3. Front wheel steering of the vehicle

At the rear axle pivot (X_r, Y_r) of the vehicle, the speed is:

$$\upsilon_r = \dot{X}_r \cos\varphi + \dot{Y}_r \sin\varphi \tag{1}$$

The kinematic constraints on the front and rear axles of the vehicle are:

$$\begin{cases} \dot{X}_f \sin(\varphi + \delta_f) - \dot{Y}_f \cos(\varphi + \delta_f) = 0 \\ \dot{X}_r \cos\varphi 0 \dot{Y}_r \sin\varphi = 0 \end{cases} \tag{2}$$

Can be obtained jointly from Eq. (1) and Eq. (2):

$$\begin{cases} \dot{X}_r = \upsilon_r \cos\varphi \\ \dot{Y}_r = \upsilon_r \sin\varphi \end{cases} \tag{3}$$

This can be obtained from the geometry of the front and rear wheels:

$$\begin{cases} X_f = X_r + l\cos\varphi \\ Y_f = Y_r + l\sin\varphi \end{cases} \tag{4}$$

From Eqs. (2), (3) and (4), the angular velocity of the pendulum can be solved:

$$\omega = \frac{\upsilon_t}{l}\tan\delta_f \tag{5}$$

In Eq. (5), ω represents the vehicle's transverse angular velocity. The steering radius R of the vehicle and the front wheel deflection angle δ_r of the vehicle can be obtained from ω and υ_t:

$$\begin{cases} R = \upsilon_r / \omega \\ \delta_f = \arctan(l / R) \end{cases} \tag{6}$$

From Eq. (3) and Eq. (5), the kinematic model of the vehicle is:

$$\begin{bmatrix} \dot{X}_r \\ \dot{Y}_r \\ \dot{\varphi} \end{bmatrix} = \begin{bmatrix} \cos\varphi \\ \sin\varphi \\ \tan\delta_f / l \end{bmatrix} \upsilon_r \tag{7}$$

The model can be further represented in a more general form:

$$\xi_{kin} = f_{kin}(\xi_{kin}, u_{kin}) \tag{8}$$

In Eq. (8), the state quantity $\dot{\xi}_{kin} = [X_r, Y_r, \varphi]^T$ and the control quantity $u_{kin} = \left[\nu_r, \delta_f\right]$. In the path planning of the vehicle and the tracking of the trajectory, $[p_r, \omega]$ is used as the control quantity of the vehicle, which is obtained from Eq. (5) and Eq. (7):

$$\begin{bmatrix} \dot{X}_r \\ \dot{Y}_r \\ \dot{\varphi} \end{bmatrix} = \begin{bmatrix} \cos\varphi \\ \sin\varphi \\ 0 \end{bmatrix} \upsilon_r + \begin{bmatrix} 0 \\ 0 \\ 1 \end{bmatrix} \omega \tag{9}$$

2.2.2. Improvement of the Fast Expanding Randomized Tree Algorithm:

1) Increase the gravitational component. The idea of artificial potential field method is introduced into the fast expansion random tree algorithm, which adds gravitational components to the two-way random tree to guide the two-way random tree to expand and grow towards the respective target point [26-27]. The main idea is to add a gravitational component to each new node generated during the expansion process of the bidirectional random tree search, i.e., a target gravitational function $G(n)$ is added to the generated new node n, which can be expressed as:

$$F(n) = R(n) + G(n) \tag{10}$$

In Eq. (10), $F(n)$ represents the guidance function for generating new nodes during the search process of the random tree, $R(n)$ is the random growth function from the new nodes, and $G(n)$ is the increased target gravity function.

The target gravity function of the fast expanding random tree algorithm $G(n)$:

$$G(n)=\rho\cdot k_p\cdot\frac{x_{goal}-x_{near}}{x_{goal}-x_{near}} \tag{11}$$

In Eq. (11), ρ is the step size, k_p is the gravitational gain coefficient, x_{goal} is the unmanned vehicle target position vector, and $\| x_g oal - x_{near} \|$.

Denotes the absolute value of the geometric distance between node x_{near} and target point x_{goal}.

The generation of new node x_{new} by the fast expanding random tree algorithm can be obtained:

$$R(n)=\rho\cdot\frac{x_{rand}-x_{near}}{\left\|x_{rand}-x_{near}\right\|} \tag{12}$$

Substituting Eq. (11) and Eq. (12), into Eq. (10) gives that

$$R(n)=\rho\cdot\frac{x_{rand}-x_{near}}{x_{rand}-x_{near}} \tag{13}$$

The formula for the generation of new nodes after the introduction of the idea of gravity is obtained from Eq. (13) as

$$x_{new}=x_{near}+\rho\cdot\left(\frac{x_{nand}-x_{near}}{\left\|x_{nand}-x_{near}\right\|}+k_p\cdot\frac{x_{goal}-x_{near}}{\left\|x_{goal}-x_{near}\right\|}\right) \tag{14}$$

The growth guidance function of each node of the bi-directional randomized tree is $F(n)$, so that the bi-directional randomized tree searches and grows in free space under the action of the gravitational component in the direction of the target.

2) Generation of Local Randomized Trees. The fast expanding random tree algorithm needs to detect obstacles in the process of generating new nodes in the free space search. This paper proposes to generate a number of random tree root nodes uniformly around the obstacle, to these root nodes, to the obstacle outside the search to expand the establishment of a number of local random trees, to increase the repulsive component of the local random tree, to guide the local random tree in the direction away from the obstacle to reduce the detection time of the obstacle, to improve the algorithm's efficiency in avoiding obstacles, and to reduce the number of iterations.

3) Increase the repulsive force component. The idea of obstacle repulsion in the artificial potential field method is introduced into the fast extended random tree algorithm to guide the local random tree to grow in the direction away from obstacles. The main idea is to increase the repulsion component for each new node generated in the process of local random tree search and expansion, i.e., an obstacle repulsion function is introduced for each new node n generated, which can be expressed as:

$$F(n)=R(n)+T(n) \tag{15}$$

In Eq. (15), $F(n)$ represents the guidance function of the random tree to generate new nodes during the search process of the local random tree, $R(n)$ is the random growth function from the new nodes, and $T(n)$ is the added obstacle repulsion function.

Obstacle Repulsion Function for Fast Expanded Random Tree Algorithm $T(n)$:

$$T(n)=\begin{cases} 0 \quad if \ p(x)>p_0 \\ \rho\cdot k_{rep}\cdot\left(\frac{1}{p(x)}-\frac{1}{p_0}\right)\frac{1}{p^2(x)}\frac{\partial(x_{near}-x_{obstade})}{\partial x_{near}} \\ if \ p(x)\le p_0 \end{cases} \tag{16}$$

In Eq. (16), k_{rep} is the repulsive gain coefficient, $p(x)$ denotes the shortest distance from the node to the obstacle, p_0 denotes the influence distance of the obstacle to the node, and $x_{obstacle}$ is the obstacle position vector.

It is obtained from the formula of the fast extended randomized tree algorithm for the new node x_{new}:

$$R(n)=\rho\cdot\frac{x_{rand}-x_{near}}{\| x_{rand}-x_{near}\|} \tag{17}$$

This can be obtained by substituting Eq. (16) and Eq. (17), into Eq. (15):

$$F(n)=\begin{cases} 0 \quad if \ p(x)>p_0 \\ \rho\cdot\dfrac{k_{rap}\cdot\left(\frac{1}{p(x)}-\frac{1}{p_0}\right)\frac{1}{p^2(x)}(x_{near}-x_{obstacle})}{\left\|x_{near}-x_{obstacle}\right\|}+ \\ \rho\cdot\dfrac{x_{rand}-x_{obstacle}}{\left\|x_{rand}-x_{near}\right\|} \quad if \ p(x)\le p_0 \end{cases} \tag{18}$$

The formula for the generation of new nodes after the introduction of the repulsion idea is obtained from Eq. (18) as:

$$x_{new}=\begin{cases} 0 \quad if \ p(x)>p_0 x_{new}+\beta \\ x_{new}+\rho\begin{cases}\dfrac{k_{new}\left(\frac{1}{p(x)}-\frac{1}{p_0}\right)\frac{1}{p^2(x)}(x_{new}-x_{new})}{\left\|x_{new}-x_{new}\right\|}+ \end{cases} \\ \left.\dfrac{x_{new}-x_{new}}{\left\|x_{new}-x_{new}\right\|}\right\} \quad if \ p(x)\le p_0 \end{cases} \tag{19}$$

The growth guidance function of each node of a randomized tree with a number of nodes around the obstacle as root nodes is $F(n)$, so that the multidirectional randomized tree searches and grows away from the obstacle in free space under the effect of repulsive force components.

2.2.3. Path optimization process:

1) Angular constraints. It is known from the kinematic modeling of the car:

$$\frac{r}{\delta}=\frac{\frac{v_c}{l}}{1+Kv_c^2} \tag{20}$$

In equation (20), $K=\frac{m}{l^2}\left(\frac{l_f}{C_f}-\frac{l_r}{C_r}\right)$ is called the stability factor. $\frac{r}{\delta}$ is called the steady state transverse pendulum angular velocity gain, also known as sensitivity.

It is obtained from equation (20):

$$\delta = \frac{r(1+Kv_c^2)}{v_c / l} \tag{21}$$

The stability factor K is an important indicator of steering stability performance, and the value of K is divided into three cases: neutral steering $(K=0)$, understeer $(K>0)$, and oversteer $(K<0)$.

We take neutral steering as the basis:

$$\frac{r}{\delta} = \frac{v_c}{l} \tag{22}$$

$$\delta = \frac{l}{R} \tag{23}$$

2) Node optimization. Node optimization is shown in Fig. 4, array A holds the feasible points of the passable path obtained by searching through the fast expanding random tree algorithm, 1 denotes the start point x_{imit}, n denotes the target point x_{goal}, $2 \sim (n-1)$ denotes the feasible points from the start point to the target point, and array B holds the new set of feasible points after deleting the redundant nodes.

The idea of the algorithm for optimizing the nodes is as follows:

(1) Add the initial point x_{init} to the new array B.

(2) Judge whether there is any obstacle between node n and node $n+1$, if not, skip node $n+1$, judge whether there is any obstacle between node n and the next node $n+2$, if there is any obstacle, add the node $n+2$ to array B, take $n+2$ as a new node, judge whether there is any obstacle between nodes $n+2$ and $n+3$, search backward, and so on, until traversing all the feasible nodes in array A.

(3) When all feasible points in array A are traversed and the search reaches the target point x_{goal}, end the search and add the target point to array B.

Array B is the set of optimized feasible points. Sequentially join array B to get the optimized path.

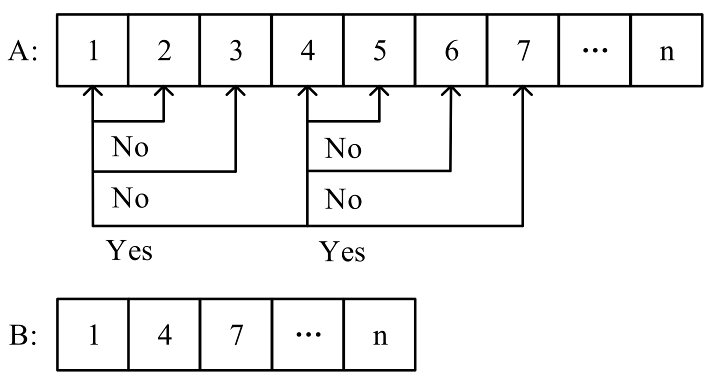

Fig. 4. Node optimization

3) Path smoothing processing. In this paper, we choose B spline curve to smooth the path generated by fast extended random tree planning.

Usually given $m+n+1$ vertex $P_i(i=0,1,2,\cdots,m+n)$, a parametric curve with $m+1$ segments and n times can be defined.The expression of B spline curve is:

$$P_{i,n}(t) = \sum_{k=0}^{n} P_{i+k} \cdot F_{k,n}(t) \tag{24}$$

In Eq. (24), $0 \le t \le 1, P_i + k\left(i = 0,1,2,\cdots,m, k = 0,1,2,\cdots,n\right)$ is the control vertex and n is the specified number of basis functions.

In the above expression $F_{k,n}(t)$ is the n times B-spline basis function, also known as the spline segmentation hybrid function, which is expressed as:

$$F_{k,n}(t) = \frac{1}{n!}\sum_{j=0}^{n-k}(-1)^j \cdot C_{n+1}^j \cdot (t+n-k-j)^n \tag{25}$$

In equation (25), $k = 0,1,2,\cdots,n$.

2.3. End-to-End Driverless Decision Model Based on Vehicle-Road Collaboration

2.3.1. Design of Group Intelligence Perception Decision Making Network Structure:

1) Modeling of related problems. The decision network model in this paper is proposed based on the premise of the above traffic scenario assumptions, and the key of the model lies in the extraction and fusion of features of the multi-vehicle group-wise sensing environment. Currently, most self-driving vehicles are loaded with sensors such as cameras, high-precision LIDAR, and millimeter-wave radar. Cameras have the advantages of low cost, high popularity, and wide application compared to other vehicle sensors, and many driver assistance functions such as panoramic parking and blind spot monitoring are currently dependent on cameras, and the autopilot proposed by the emerging car manufacturer Tesla Inc. is also a visual perception scheme based on cameras. Therefore, in this paper, the image data perceived by the vehicle is selected to be fused and processed, and the unmanned vehicle driving path is outputted by a decision algorithm.

Essentially, the problem can be described as constructing a mapping relationship from multi-vehicle group wise sensing image information to vehicle steering angle. Since the vehicle steering angle is a continuous variable, the problem can also be viewed as a regression-valued problem mention. The problem can be decomposed into two sub-problems, one is the feature extraction and fusion of multi-vehicle group wise sensory image information. The second is the mapping of fused features to vehicle steering angles. The above two sub-problems can be formally described as the following equations:

$$F:\{(x_1,x_2,\dots,x_n)^i, x_n \in T\} \to R \tag{26}$$

$$D:\{(e_1,e_2,\dots,e_r)^i, e_r \in R\} \to \{s_i, s_i \in S\} \tag{27}$$

F denotes the mapping relationship of the perception module. At moment i, the multi-vehicle image information tensor $(x_1,x_2,\dots,x_n)^i$ collected by the on-board sensors is mapped into the road environment high-dimensional feature space R after feature extraction, T denoting the image information space, and D denoting the mapping relationship of the decision module. At moment i, the decision module requests a current moment road high-dimensional environment feature tensor $(e_1,e_2,\dots,e_r)^i$ from R, (e_r denotes the requested local road environment feature of the r th vehicle under the coverage of the current roadside unit) mapped into a control parameter space S of the vehicle, s_i being a vehicle control parameter.

2) General structure of the network model. The overall structure of the model proposed in this paper is shown in Fig. 5, and this structure can be explained from two perspectives. From the vehicle's perspective, the vehicle sends the road image information collected by the camera to the edge device to request a driving decision through the vehicle-road wireless communication, and then the edge device returns the decision-making vehicle control parameters to the vehicle, which is completely an end-to-end process for the vehicle.

From the perspective of the edge device, the edge device receives the road image information from the vehicle and extracts the local features of the road environment using the perception module.

Then, according to whether the vehicle requests a driving decision or not, the local features are further fused to generate a driving decision and return it to the vehicle or the local features are cached in the road environment feature database. At the same time, the edge device needs to upload the local road environment feature database to the algorithm training platform in the cloud for iterative algorithm update training to strengthen the performance of the algorithm.

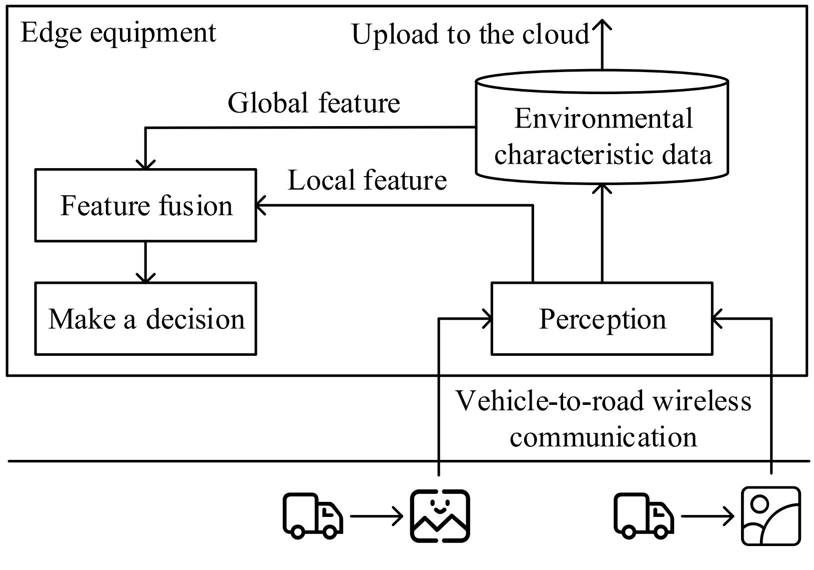

Fig. 5. Group intelligent perception driving decision model framework

2.3.2. Vehicle-Road Collaboration Group Intelligence Perception Decision Algorithm:

1) Groupwise perceptual decision-making network model structure. A multilayer convolutional network is utilized in the perceptual network for high-dimensional feature extraction of the input road image data. Through the setting of the number of convolution kernels, the original input image data of three dimensions (image color RGB channel), the dimension becomes tens of dimensional data, and the high-dimensional feature information is extracted. At the same time, by setting the convolution step size and convolution kernel size (generally 3*3) of the convolution layer and adding a pooling layer, the image size becomes smaller with the deepening of the number of layers, and is eventually reduced to a feature subgraph composed of individual pixels. The high-dimensional feature information is then stored in each dimension, and the feature value of a dimension represents a specific road semanticization information.

The fusion decision network can be regarded as a dimensionality reduction process for high-dimensional features, by setting up multi-layer fully connected layers, increasing the complexity of the decision network to improve the learning ability of the network and decreasing the dimensionality of the features layer by layer, and finally reducing the dimensionality of the output into the size of the result, a real number. Through network training, find the weights of each dimensional feature, and map the high-dimensional features into a final continuous variable value. At the same time set to set a nonlinear activation function for each layer of neurons, which is conducive to the decision network to fit more complex high-dimensional features. In this paper, the decision network uses the ReLU activation function, which has a more stable gradient and faster convergence compared to the sigmoid function. While the sigmoid is very smooth after the output value is greater than 0.9, the gradient is easily disappeared in the deep neural network.

2) Optimization objective and parameter update:

(1) Cost function. The problem solved by the algorithm is actually the prediction of vehicle steering angle control parameters, and the optimization objective of the model is to make the steering angle values predicted by the network differ from the actual steering angle values. In

general, the optimization objective is formally described as a loss function during training, defined as: $L_\theta(y_i, \hat{y}_i)$, i.e., a function of the predicted value y_i and the true value $\hat{y}_i$ under parameter θ, and the loss function is adjusted to reach the optimal solution by adjusting parameter θ. In this paper, since the model is trained end-to-end and the output of the model is a continuous variable, there are generally two functions for measuring the model error for a continuous variable: mean square error (MSE), root mean square error (RMSE), and mean absolute error (MAE), which are given by the following formulas (where the function h denotes the mapping relationship of the model, m is the capacity of the data samples, $x^{(i)}$ is the data samples, and $y^{(i)}$ is the data sample (the labeling value of the data sample):

$$MSE(x,h) = \frac{1}{m}\sum_{i=1}^{m}(h(x^{(i)}) - y^{(i)})^2 \tag{28}$$

$$MAE(x,h) = \frac{1}{m}\sum_{i=1}^{m}| h(x^{(i)}) - y^{(i)} | \tag{29}$$

From the above equation it can be seen that the MSE equation is the sum of the squared terms, while the MAE calculates the absolute error value, the two in comparison MSE can amplify the impact of outliers on the optimization network. In this paper, MSE is used as the cost function (defined in the following equation), where θ is the parameter that needs to be learned for the training of the network model:

$$L(x^{(i)};\theta) = \frac{1}{m}\sum_{i=1}^{m}(h_\theta(x^{(i)}) - \hat{y}^{(i)})^2 \tag{30}$$

(2) Parameter update method. The network model in this paper is trained using the back-propagation algorithm. The parameter updating algorithm is an updating process that enables the gradient of the cost function to approximate the optimal value faster and more efficiently by adjusting the θ parameters. The parameter updating algorithm used in this paper is Adaptive Moment Estimation (Adam), which is a first-order optimization algorithm that evolved from Stochastic Gradient Descent (SGD) and can be used in place of Stochastic Gradient Descent (SGD), and combines the advantages of Adaptive Gradient Algorithm (AdaGrad) and Root Mean Square Propagation Algorithm (RMSProp).SGD is very much applied in deep neural network training and is capable of avoiding the training network from falling into local optimal solutions. can avoid training the network to fall into local optimal solution, but it is difficult to set the initial value of the learning rate, in the training process for each parameter are used for the same learning rate, can not be targeted to adapt to the changes of each parameter.Adam related parameter update formula is shown below, β_1 is the exponential decay coefficient, control the current gradient and momentum, initialized to the value of close to 1, β_2 coefficients are the exponential decay rate, control the the effect of the previous squared value of the gradient. It is necessary to explain the algorithmic process of Adam in order to familiarize ourselves with the training process of the model:

$$g_t = \nabla_\theta J(\theta_{t-1}) \tag{31}$$

$$m_t = \beta_1 m_{t\text{-}1} + \frac{(1-\beta_1)}{g_t} \tag{32}$$

$$v_t = \beta_2 v_{t-1} + \frac{(1-\beta_2)}{g_t^2} \tag{33}$$

$$\hat{m}_t = \frac{\hat{m}_t}{(1-\beta_1^t)} \tag{34}$$

$$\hat{v}_t = \frac{\hat{v}_t}{(1-\beta_2^t)} \tag{35}$$

$$\theta_t = \theta_{t-1} - \eta \cdot \frac{\hat{m}_t}{(\sqrt{\hat{v}_t} + \varepsilon)} \tag{36}$$

3. Model validation

3.1. Comparison of path optimization results

3.1.1. Comparison of optimization results. The design of two adjacent intersections i and j with intersection spacing of 500 meters, intersection inlet knife numbering, lane function division and phase phase sequence are shown in Figure 6.

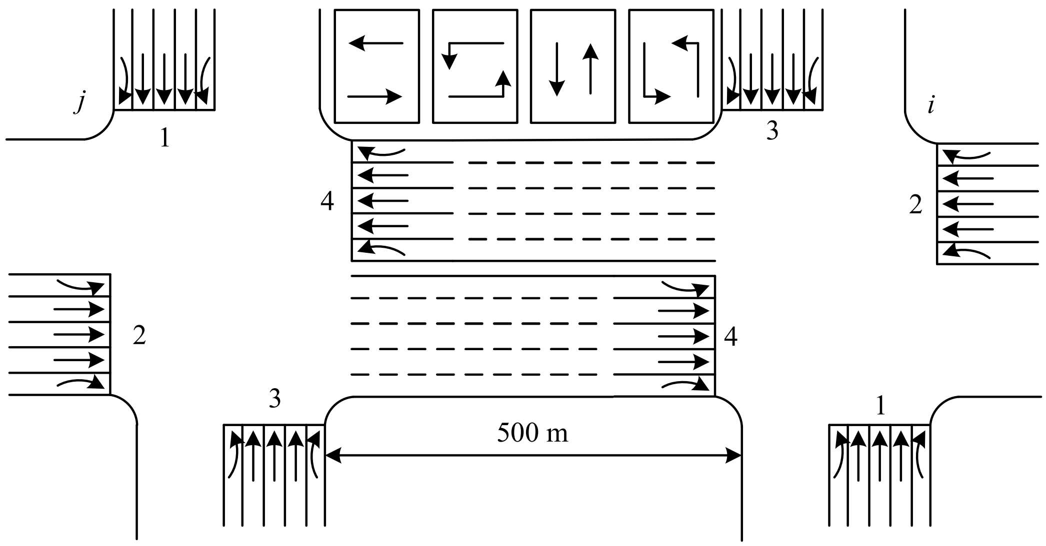

Fig. 6. Basic layout of the study area

Set the common coordination cycle of the two intersections as 130s, the total loss time of each cycle as 13s, and the saturation flow rate as 2000cpu/h, then the saturation headway spacing is 2.5s. Set the reasonable speed change range of the roadway traffic flow as 4.5-14.5m/s (16.2-52.2km/h), and the transmission speed of the start-up wave as 5m/s, and the average headway spacing of queuing vehicles as 7.5 m. The green time is allocated according to the saturation degree of each inlet road, and the saturation degree of each intersection inlet road is set to 0.8.

The path flow distribution and signal timing of the two intersections are shown in Figure 7. In this case, the coordination parameters for each path are calculated as shown in Table 1. Where, t1 (t2) is the length of time that traffic exits at saturated flow (unsaturated flow) for path coordination phase at intersection i, Q1 (Q2) is the number of vehicles in the path saturated flow (unsaturated flow) traffic, T is the length of green light required to clear the initial queue for the path coordination phase at the intersection, g1 (g2) is the length of time that the effective green light period is used for the initial queue clearance at the path coordination phase at intersection j to serve saturated (unsaturated) traffic during the green light period.

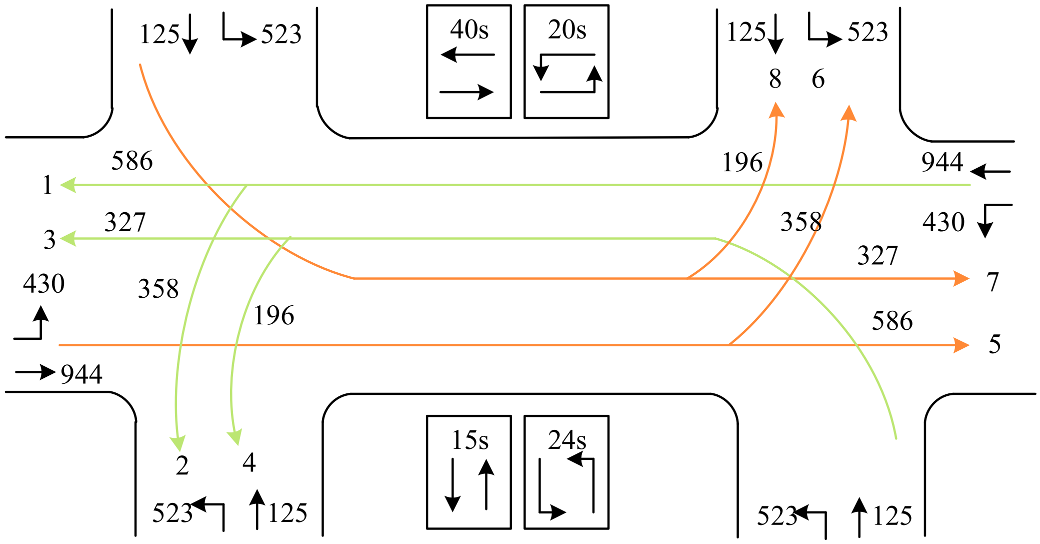

Fig. 7. Traffic volumes for each route and signal timing

Table 1. Parameter for each route

Parameter	Optimized routes							
	1	2	3	4	5	6	7	8
t1	25	25	15	15	25	25	15	15
t2	14	14	7	7	14	14	7	7
Q1	15	8	10	4	15	8	10	4
Q2	3	2	1	0	3	2	1	0
T	40	20	60	40	40	20	60	40
g1	25	13	27	13	25	13	27	13
g2	14	6	12	6	14	6	12	6

In order to verify the effectiveness of the model in this paper, the empirical analysis compares the optimization effect of three schemes. Scheme 1: Maxband optimization scheme. Scheme 2: Synchro optimization scheme. Scheme 3: The optimization scheme of this paper's model.

In Scheme 1 and Scheme 2, the driving speed of the road section is set to the maximum value of 14.5m/s, and the comparison results are shown in Table 2. As can be seen from Table 2, the optimized paths of this paper's model are path 1 and path 7, while both Scheme 1 and Scheme 2 optimize the main flow to path 1 and path 5, and the phase difference of each model optimization is different. In terms of driving speed, the optimization result of Scheme 3 of this paper's model is equal to the maximum speed. By comparing the waiting time for red light, it can be seen that the waiting time for red light in two directions of this model is 10s and 8s respectively, which is obviously shorter than that of Scheme 1 and Scheme 2. This model can greatly improve the efficiency of the optimized path vehicles through. The comparison of green wave bandwidth, waiting time for red light, and passing efficiency value of the optimized path is shown in Figure 8.

From Fig. 8(a), it can be seen that the Maxband scheme and the Synchro scheme have the same width of bandwidth in both directions, while the model optimization scheme in this paper can significantly improve the green wave bandwidth, comparing the Maxband scheme and the Synchro scheme, the present scheme improves the green wave bandwidth by 157% and 93% in direction i→j, respectively. The scheme in this paper improves the green wave bandwidth by 76% and 133% in direction j→i, respectively. The total bandwidth improvement is 113% in both directions. The reason why this paper's model can significantly improve the green wave bandwidth is to optimize the bi-directional path 1 and path 7, while the Maxband scheme and Synchro scheme optimize the bi-directional mainstream direction path 1 and path 5. The disadvantage of bi-directional optimization of the mainstream direction is that the effectiveness of optimization in this direction will negatively affect the optimization of the other direction, and this paper's model circumvents this shortcoming through the optimization of coordinated paths.

From Fig. 8(b), it can be seen that comparing the Maxband scheme with the Synchro scheme, the optimized path of this paper's model has a short waiting time for red lights, which is significantly lower than the rest of the schemes.

From Fig. 8(c), it can be seen that the passing benefit values of this paper's model are significantly higher than those of the Maxband scheme and the Synchro scheme, regardless of direction j→i or direction i→j. On the bi-directional optimization path, although both the Maxband scheme and the Synchro scheme coordinate the main flow direction with the highest flow rate, the model in this paper has the highest passing benefit value, which is 70.3% and 46.8% higher than the Maxband scheme and the Synchro scheme, respectively.

Table 2. Comparison of results

Scheme		1	2	3
Direction: i→j	Optimized route	1	1	1
	Phase difference/s	0	6	25
	Driving speed/($m \cdot s^{-1}$)	14.5	14.5	14.5
	Time for red light/s	32	26	10
Direction: j→i	Optimized route	5	5	7
	Phase difference/s	0	120	32
	Driving speed/($m \cdot s^{-1}$)	14.5	14.5	14.5
	Time for red light/s	29	23	8

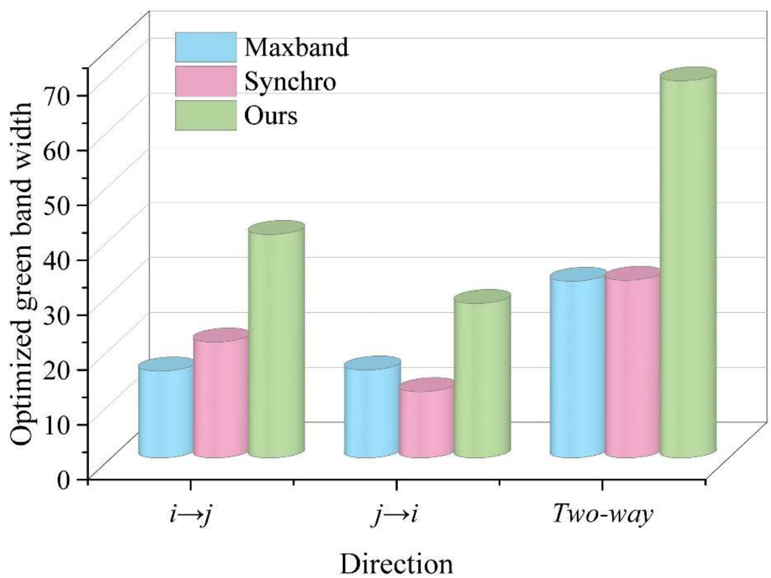

(a) Comparison of green band width for different models

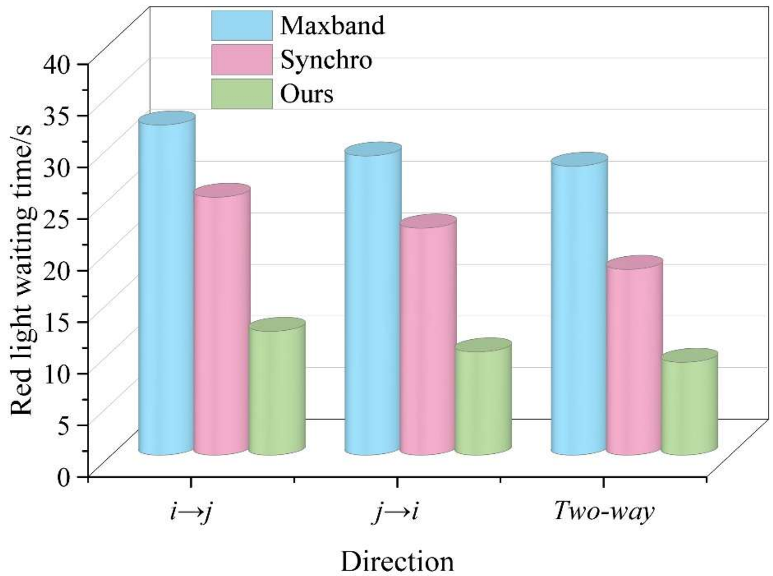

(b) Comparison of red light waiting time for different models

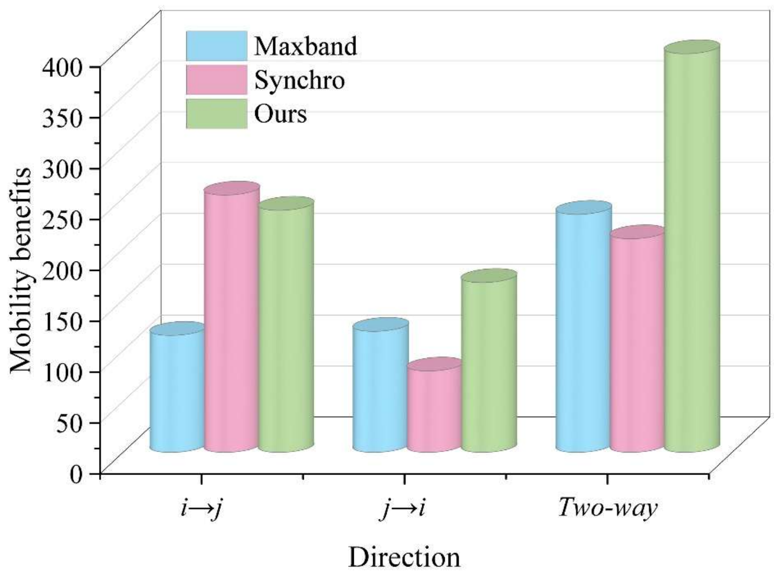

(c) Comparison of mobility benefits for different models

Fig. 8. Comparison of different models

3.1.2. Path optimization simulation. In order to further verify the effectiveness of the model in this paper, this subsection will take the driving perspective of the main vehicle as a reference to construct a scene in which the main vehicle is driving at an intersection to further verify the effectiveness of the algorithm in this paper. Referring to relevant data, it is found that vehicles at intersections are most likely to have accidents when turning right, therefore, simulations are conducted for the right-turn path at intersections, and the function of the main vehicle's right-turn is tested in a random traffic flow.

In the intersection in the previous Figure 6, several vehicles attempt to drive from the left intersection of intersection i to the right intersection, and the main vehicle will interact with them during the right turn. At the same time, some of the vehicles are located on one side of the intersection at the same time as the main vehicle and randomly drive in other directions of the intersection. In addition, the vehicles on the upper side of the intersection also randomly drive to other intersections.

The velocity profile and path of the main vehicle turning right at the intersection are shown in Fig. 9, Fig. 9(a) shows the velocity profile of the right turn, and Fig. 9(b) shows the right turn path planned by the model. From Fig. 9(a), it can be seen that the main vehicle shows a general trend of acceleration. From Fig. 9(b), it can be seen that during the whole simulation process, the main vehicle roughly completes the right-turn action along the right-turn lane, and its path does not deviate from the center of the lane, and the path planning performance is excellent.

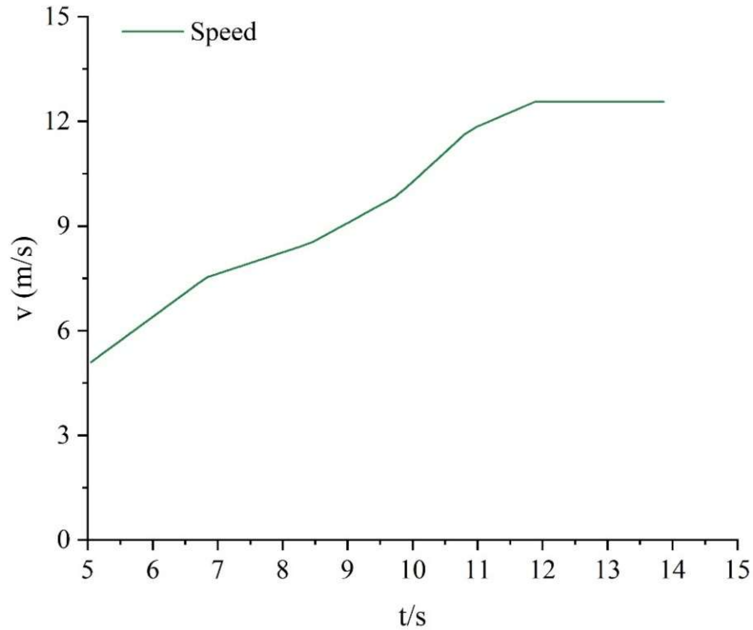

(a) Speed curve

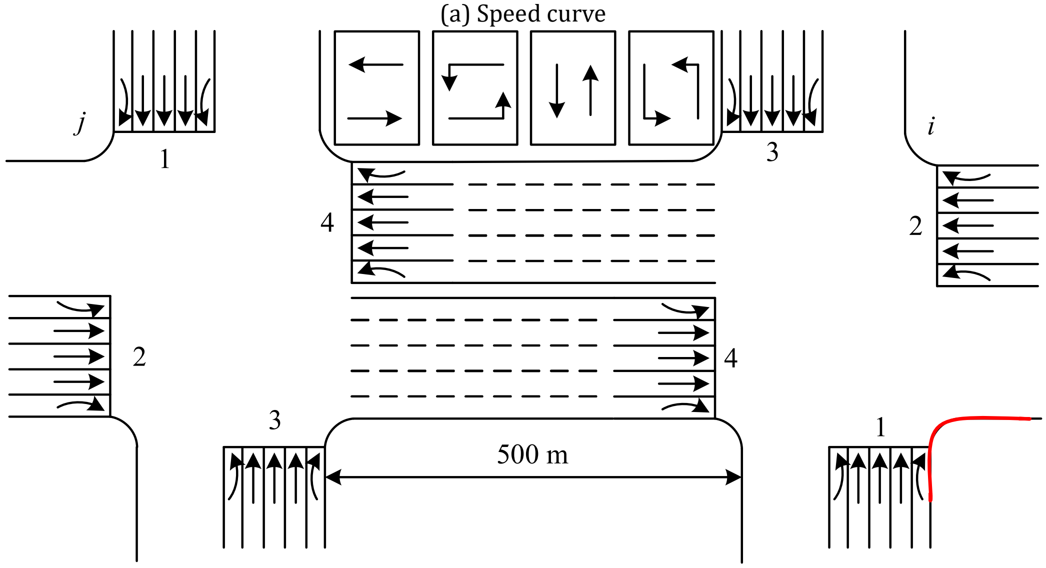

(b) Optimized route

Fig. 9. Speed curve and route of main car

3.2. Decision Modeling Path Planning Traveling Cost Analysis

The cost of the driving path planned by the unmanned decision model in this paper is analyzed, and the relationship between speed and driving consumption is used to calculate the fuel consumption, and the variation of the value of the unmanned vehicle's normative driving speed will not only have an impact on the driving time, but also on the fuel consumption. Now, 20 is defined as the baseline speed value of unmanned vehicle normal traveling. In this section, the normal driving speed is analyzed in detail, and the number of defaults, fuel consumption, CO2 emissions, and distribution costs are compared for 25 different values of normal driving speed under the same scale. The specific data is shown in Table 3.

From the data in Table 3, it can be found that:

1) When the value of the normal driving speed is taken at [14,38], the fuel consumption of the

driverless vehicle shows obvious fluctuation up and down oscillation. In this case, the fuel consumption is calculated based on the relationship between fuel consumption and speed, and the change of road conditions will cause the speed to change. Due to the small driving range, the difference in fuel consumption at each value of the normal driving speed is less obvious.

2) When the value of normal driving speed is taken at [14,38], the trend of CO2 emissions of the driverless vehicle fluctuates roughly with the fuel consumption.

3) When the value of normal driving speed is taken at [14,38], the total cost of driving decreases more significantly as the normal driving speed increases. When the value is [29,38], there is a small increase in the trend of the folded line, but it does not change the overall decreasing trend.

Table 3. Driving cost in different normal driving speed

Normal speed value	Fuel consumption	Carbon dioxide emission	Total driving cost
14	1.985	3.326	16.72
15	1.935	3.184	16.13
16	1.922	3.012	15.92
17	1.374	2.982	14.54
18	1.162	2.964	12.56
19	1.253	2.826	11.24
20	0.994	2.647	9.08
21	0.994	2.538	8.94
22	0.958	2.495	9.02
23	0.954	2.495	8.93
24	0.997	2.334	8.84
25	0.997	2.327	8.57
26	0.892	2.156	7.96
27	0916	2.166	7.93
28	0.983	2.394	8.06
29	1.264	2.402	9.03
30	1.203	2.596	9.49
31	1.275	2.713	9.62
32	1.122	2.694	9.73
33	1.122	2.806	9.84
34	1.287	3.116	10.65
35	1.521	2.946	9.94
36	1.688	3.044	10.22
37	1.594	3.227	10.74
38	1.653	3.362	10.87

4. Conclusion

In this paper, we model the kinematics of the driverless car and optimize the driving path of the driverless car by improving the fast extended random tree algorithm. The swarm intelligence perception decision-making algorithm is used to construct an end-to-end driverless decision-making model based on vehicle-circuit coordination.

1) The waiting time for red light in this paper's model is the minimum among all the schemes. The model in this paper can significantly improve the passing efficiency of vehicles in the optimized path and significantly improve the green wave bandwidth. Compared with other schemes, the two-way of this paper's model improves the bandwidth by a total of 113%. The passing efficiency values of this

paper's model are improved by 70.3% and 46.8% over the Maxband scheme and Synchro scheme, respectively.

2) In the unmanned vehicle right turn simulation scenario, the main vehicle shows a general trend of acceleration and the path does not deviate from the center of the lane, which is a good optimization effect.

3) The fuel consumption of the unmanned vehicle fluctuates up and down when the normal driving speed takes the value of [14,38]. The trend of CO2 emissions of the unmanned vehicle is roughly in line with the fuel consumption. The total cost of traveling decreases with increasing speed.

Funding

This research was supported by the “Research and Demonstration of Key Technologies for Construction, Operation and Maintenance of Digital Highways Based on 5G and Artificial Intelligence”; Program Category: Major Science and Technology Special Program, Project No. 202102AD080003.

References

[1] Zhang, X., Gao, H., Guo, M., Li, G., Liu, Y., & Li, D. (2016). A study on key technologies of unmanned driving. CAAI Transactions on Intelligence Technology, 1(1), 4-13.

[2] Park, J., & Kang, D. (2017). Trend analysis of unmanned technology using patent information. Journal of The Korea Society of Computer and Information, 22(3), 89-96.

[3] Edwards, D. J., Akhtar, J., Rillie, I., Chileshe, N., Lai, J. H., Roberts, C. J., & Ejohwomu, O. (2022). Systematic analysis of driverless technologies. Journal of engineering, design and technology, 20(6), 1388-1411.

[4] Koul, S., & Eydgahi, A. (2018). Utilizing technology acceptance model (TAM) for driverless car technology adoption. Journal of technology management & innovation, 13(4), 37-46.

[5] Yu, L., Wang, X., Hou, Z., Du, Z., Zeng, Y., & Mu, Z. (2021). Path planning optimization for driverless vehicle in parallel parking integrating radial basis function neural network. Applied Sciences, 11(17), 8178.

[6] Leng, K., & Li, S. (2021). Distribution path optimization for intelligent logistics vehicles of urban rail transportation using VRP optimization model. IEEE Transactions on Intelligent Transportation Systems, 23(2), 1661-1669.

[7] Zhongrui, Y., Houyu, Y., & Miaohua, H. (2017, December). Improved ant colony optimization algorithm for intelligent vehicle path planning. In 2017 International Conference on Industrial Informatics-Computing Technology, Intelligent Technology, Industrial Information Integration (ICIICII) (pp. 1-4). IEEE.

[8] Zhou, C., Gu, S., Wen, Y., Du, Z., Xiao, C., Huang, L., & Zhu, M. (2020). The review unmanned surface vehicle path planning: Based on multi-modality constraint. Ocean Engineering, 200, 107043.

[9] Ayawli, B. B. K., Chellali, R., Appiah, A. Y., & Kyeremeh, F. (2018). An Overview of Nature - Inspired, Conventional, and Hybrid Methods of Autonomous Vehicle Path Planning. Journal of Advanced Transportation, 2018(1), 8269698.

[10] Zhu, D. D., & Sun, J. Q. (2021). A new algorithm based on Dijkstra for vehicle path planning considering intersection attribute. IEEE Access, 9, 19761-19775.

[11] Oubbati, O. S., Atiquzzaman, M., Lorenz, P., Baz, A., & Alhakami, H. (2020). SEARCH: An SDN-enabled approach for vehicle path-planning. IEEE Transactions on Vehicular Technology, 69(12), 14523-14536.

[12] Guvenc, L., Aksun-Guvenc, B., Zhu, S., & Gelbal, S. Y. (2021). Autonomous Road Vehicle Path Planning and

Tracking Control. John Wiley & Sons.

[13] Wang, Y., Jiang, J., Li, S., Li, R., Xu, S., Wang, J., & Li, K. (2023). Decision-making driven by driver intelligence and environment reasoning for high-level autonomous vehicles: a survey. IEEE Transactions on Intelligent Transportation Systems, 24(10), 10362-10381.

[14] Li, L., Ota, K., & Dong, M. (2018). Humanlike driving: Empirical decision-making system for autonomous vehicles. IEEE Transactions on Vehicular Technology, 67(8), 6814-6823.

[15] Zheng, X., Huang, H., Wang, J., Zhao, X., & Xu, Q. (2021). Behavioral decision‐making model of the intelligent vehicle based on driving risk assessment. Computer‐Aided Civil and Infrastructure Engineering, 36(7), 820-837.

[16] Wang, X., Shi, H., & Zhang, C. (2020). Path planning for intelligent parking system based on improved ant colony optimization. IEEE Access, 8, 65267-65273.

[17] Li, T., He, Z., & Wu, Y. (2022). An integrated route planning approach for driverless vehicle delivery system. PeerJ Computer Science, 8, e1170.

[18] Ma, H., Pei, W., & Zhang, Q. (2022). Research on path planning algorithm for driverless vehicles. Mathematics, 10(15), 2555.

[19] Wang, X., Gao, Y., Zhou, J., & Wu, H. (2023). Mini-Review of Unmanned Vehicle Route Planning Based on Ant Colony Algorithm. Automation and Machine Learning, 4(2), 42-46.

[20] Lu, J. (2021, October). Automatic Shortest Path Planning Method for Driverless Vehicles Based on Improved Ant Colony Algorithm. In 2021 3rd International Conference on Artificial Intelligence and Advanced Manufacture (pp. 1591-1595).

[21] Zhang, J., Liao, Y., Wang, S., & Han, J. (2017). Study on driving decision-making mechanism of autonomous vehicle based on an optimized support vector machine regression. Applied Sciences, 8(1), 13.

[22] Wang, X., Qi, X., Wang, P., & Yang, J. (2021). Decision making framework for autonomous vehicles driving behavior in complex scenarios via hierarchical state machine. Autonomous Intelligent Systems, 1, 1-12.

[23] Chen, X. M., Jin, M., Miao, Y. S., & Zhang, Q. (2017). Driving decision-making analysis of car-following for autonomous vehicle under complex urban environment. Journal of central south university, 24, 1476-1482.

[24] Xu, C., Zhao, W., & Wang, C. (2019). An integrated threat assessment algorithm for decision-making of autonomous driving vehicles. IEEE transactions on intelligent transportation systems, 21(6), 2510-2521.

[25] Wenchao Yan,Hua Cao,Jiazhong Chen & Tao Wu. (2024). FETR: Feature Transformer for vehicle-infrastructure cooperative 3D object detection. Neurocomputing128147-128147.

[26] Yaozhe Zhou,Yujun Lu & Liye Lv. (2024). GVP-RRT: a grid based variable probability Rapidly-exploring Random Tree algorithm for AGV path planning. Complex & Intelligent Systems(prepublish),1-14.

[27] Zhuo Huang,Yang Gao,Jian Guo,Chen Qian & Qingwei Chen. (2024). An adaptive bidirectional quick optimal Rapidly-exploring Random Tree algorithm for path planning. Engineering Applications of Artificial Intelligence108776-.